Compton Imaging with the *Daksha* Space Telescope

B.Tech Project II

Advait Mehla
Guides : Prof. Gulab Dewangan, IUCAA Pune
Prof. Varun Bhalerao, IIT Bombay

Abstract

The proposed high-energy mission *Daksha* will continuously monitor the entire sky in the 1 - 1000 keV range with unprecedented sensitivity. The mission will contain an arrangement of 17 Medium Energy Packages consisting of a total of 340 Cadmium Zinc Telluride (CZT) detectors, sensitive in the 20-200 keV range. 13 of these are placed in a quasi-hemispherical arrangement, creating a dome - inside which are 4 High Energy Packages. These consist of Sodium Iodide (NaI) scintillators read by arrays of Silicon Photomultipliers (SiPMs) to cover the 100 keV - 1000 MeV energy range. Together, this geometry of detectors presents a unique opportunity to use *Daksha* as a Compton imager with all-sky sensitivity. This imaging method relies on the nature of Compton kinematics - where, given the incident and scattered photon energies, it is possible to localize rings of likely origin in the sky for each scattering event that is detected, known as 'event circles'. These scattering events can be detected by isolating pairs of coincident events across detectors. With the detection of enough such pairs, it is possible to find the intersection of many event circles and hence successfully localize sources in the sky. Although the X-ray background dominates over most persistent sources for short exposures, integrating over timescales on the order of the five year mission lifetime could yield enough data to develop an all-sky map in the sub-MeV energy range, which would be the first of its kind. In this work, I will discuss results from extensive simulations of the *Daksha* mass model and detail the methodology used to reconstruct sources.

Contents

1 Daksha **4**

1.1 ME Packages 4

1.2 HE Packages 5

2 Mass Model **5**

3 Compton Imaging **6**

3.1 Other Missions 6

3.1.1 CGRO/COMPTEL 7

3.1.2 INTEGRAL/IBIS 7

3.2 COSI 8

3.3 Potential with Daksha 8

4 Simulations **8**

5 Methodology **9**

5.1 Event Selection 9

5.2 Error due to energy resolution 11

5.3 Error due to position resolution 11

5.4 Reconstruction 12

5.5 Visualization 12

6 Compton Data Space **13**

6.1 Angular Resolution 14

7 Simulating Crab Nebula **15**

7.1 Compton Data Space Analysis 16

7.2 Angular Resolution 17

7.3 Back-projected Images 19

8 Including Background **20**

8.1 Simulations 20

8.2 Detected Background due to Photons 21

8.3 Detected Background due to Particles 22

9 Conclusion and Future Work **22**

10 Acknowledgements **23**

1 Daksha

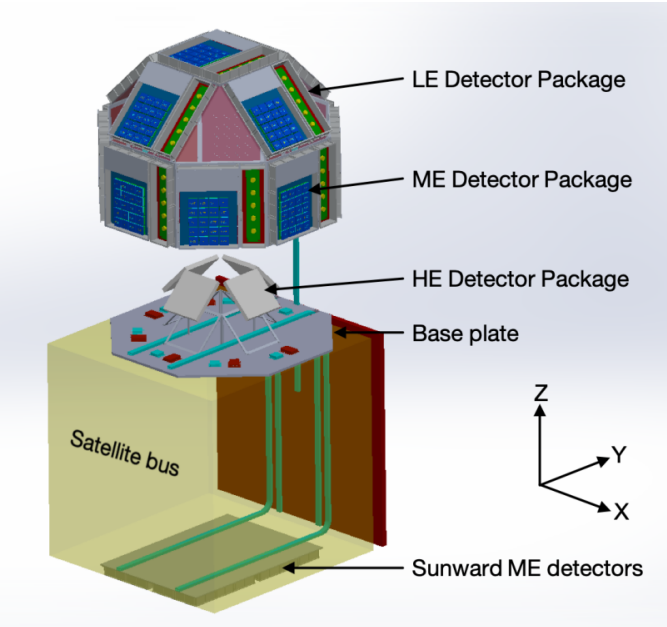

Figure 1: Design of a *Daksha* satellite. Source: Bhalerao et al. (2022)

Daksha is a proposed space telescope being developed by several Indian research institutes, with IITB leading the efforts. It will be an order of magnitude more sensitive than any existing mission. It will cover the energy range from 1 keV to 1 MeV, reaching a sensitivity higher than the Neil Gehrels Swift Observatory. Two satellites orbiting on opposite sides of Earth will ensure continuous coverage of the entire sky. The dome shaped payload has 13 surfaces, each carrying Low-energy (LE) and Medium-energy (ME) detector packages. Four ME packages are mounted under the satellite bus, and always point at the sun. Four High-energy (HE) detector packages are mounted inside the dome, along with processing electronics. (Bhalerao et al., 2022). In this work, we are concerned with events where an ME detector acts as the scatterer while an HE detector is the absorber.

1.1 ME Packages

The workhorse for *Daksha* are sensitive pixelated Cadmium Zinc Telluride (CZT) detectors. *Daksha* will use 3.9 cm$\times$3.9 cm$\times$5 mm detectors, sensitive to an energy range of $20 - 200$ keV. Each individual detector is divided into a 16$\times$16 pixel array. Medium Energy (ME) packages will consist of 20 such detectors, and *Daksha* will have 17 such ME packages. These detectors have a time resolution of 1 μs and energy resolution of 10%.

1.2 HE Packages

Each HE package consists of a 20 cm×20 cm×5 cm NaI(Tl) crystal scintillator read out by an array of Silicon Photomultipliers (SiPMs). Thes are sensitive to the 100 keV - 1 MeV energy range. The HE packages have a time resolution of 10 μs and energy resolution of 7%. Additionally, the SiPMs have a position resolution of 1 cm, and there shall be a 20×20 array of these to cover the entire crystal.

2 Mass Model

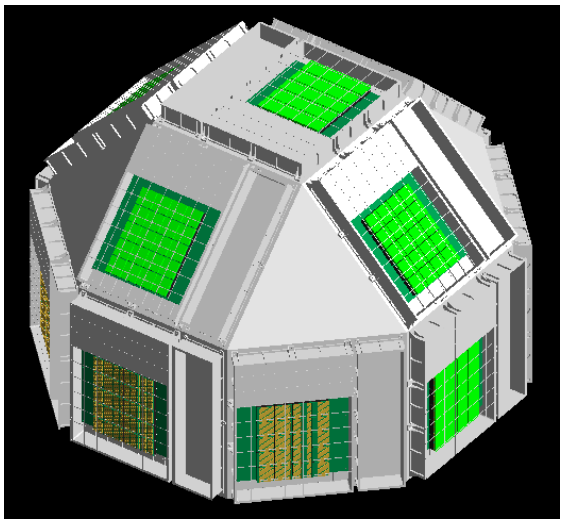

Figure 2: The *Daksha* dome with 13 ME packages mounted.

The *Daksha* mass model is used to realistically simulate the interaction of photons with the satellite and determine the counts received by every pixel of every detector onboard. The mass model is an accurate replication of the structure, geometry and chemical composition of the entire satellite. Simulations are done using GEANT4[1] (Agostinelli et al., 2003), a Monte Carlo simulation toolkit to simulate particle-matter interactions developed by CERN. GEANT4 supports a diverse set of physical processes and interactions from the eV to GeV range, including support for polarised sources, customized source planes, energy spectra etc. Data from these simulations is used to determine polarisation sensitivity and for developing and testing the polarisation pipeline.

[1] https://geant4.web.cern.ch/

3 Compton Imaging

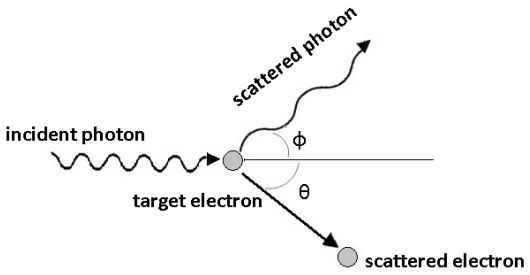

Figure 3: Kinematics of Compton scattering. Source: Venugopal & Bhagdikar (2013)

The technique of Compton imaging relies on the kinematics of Compton scattering. When a photon scatters off an electron, the scattered photon can be emitted in any direction. However, there is a relationship between the energies of the incident and scattered photons (E_γ and E_γ' respectively), and the scattering angle (ϕ). This relationship is given by the Compton formula:

$$\frac{1}{E'_\gamma} - \frac{1}{E_\gamma} = \frac{1}{m_e c^2}(1 - \cos\phi) \tag{1}$$

Here, m_e is the mass of the electron. It is important to note that E_γ, the energy of the incident photon is unknown. In events where the incident photon undergoes a Compton scatter in the ME detector and subsequently photoabsorbed in the HE dector, E_γ can be determined from the sum of the two energy deposits. This is, of course an ideal case. In reality, the second interaction could also be Compton, or both interactions could simply be uncorrelated chance coincidences.

Therefore, given the magnitude of energy deposits, the scattering angle can be determined. Given the location of both the events, the direction vector of the scattered photon can be found. These two pieces of information can be used to constrain the incident photon vector to a cone. Projected to the sky, this vector limits the possible origin of the photon to a ring on the sky, known as the 'event circle'. The intersection of many such event circles can be used to determine the location of the source.

3.1 Other Missions

The Compton imaging method is the most efficient way to image the sky in the MeV range, and has been used by missions in the past to achieve similar goals. The most notable of these are the *Compton Gamma Ray Observatory* (CGRO) and *INTEGRAL*.

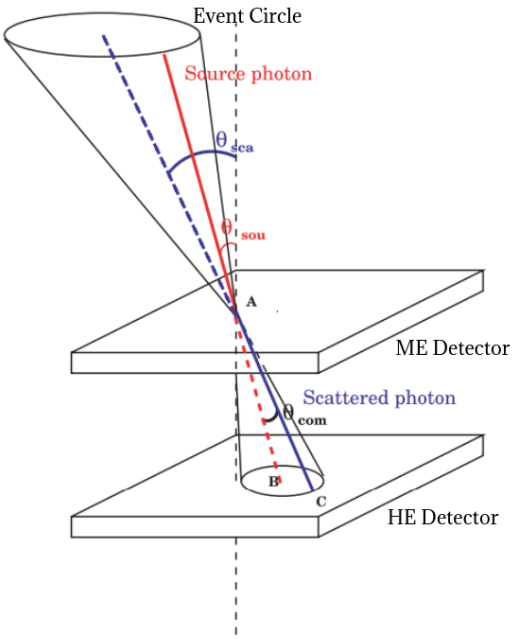

Figure 4: Diagram showing an event circle. Adapted from Forot et al. (2007)

3.1.1 CGRO/COMPTEL

The imaging Compton telescope, or COMPTEL (Schönfelder et al., 1984) was one of the four instruments on-board NASA's *Compton Gamma Ray Observatory (CGRO)* mission launched in 1991. It was designed to be sensitive in the 1 – 30 MeV range, which is part of the relatively unexplored 'MeV gap'. The instrument consisted of two layers of detectors separated by 1.5m. The upper layer, D1 consists of a liquid scintillator while the lower layer, D2 had NaI crystals. The instrument had a field of view of 1 sr and an angular resolution of $\sim 5^{\circ}$.

COMPTEL was active for 9 years, and made many notable discoveries, with several continuum all-sky maps in the MeV range, along with the first all-sky map of the 1.8 MeV line from radioactive ^{26}Al decay (Knödlseder et al., 1999), a tracer of nucleosynthesis in the galaxy.

3.1.2 INTEGRAL/IBIS

The *International Gamma-Ray Astrophysics Laboratory (INTEGRAL)* was launched in 2002 and carried the next major iteration of a Compton imager, IBIS (Forot et al., 2007). This instrument was sensitive in the 15 keV - 10 MeV range, and similarly consisted of two layers of detectors, called ISGRI and PICsIT. ISGRI was composed of CdTe detectors sensitive in the 15 keV - 1 MeV range, while PICsIT consisted of

CsI detector sensitive in the 0.2 - 10 MeV range. One key difference is that IBIS had a coded aperture mask over ISGRI, making it the first Coded Aperture Compton Telescope (CACT). This enabled it to operate at a much better angular resolution of $12'$ over a $29^\circ \times 29^\circ$ FOV.

3.2 COSI

The Compton Spectrometer and Imager (COSI) is a Small Explorer (SMEX) mission concept proposed under the Astro2020 Decadal Survey on Astronomy and Astrophysics. It is a wide-field Compton survey telescope designed to be sensitive in the $0.2 - 5$ MeV energy range, which is an unexplored region of the MeV gap. COSI uses a new, compact Compton telescope design that relies on a stacked array of germanium strip detectors to accurately track and reconstruct events that undergo multiple Compton scatters inside the instrument. These detectors are capable of precise energy and position measurements, giving COSI significant improvements in sensitivity, spectral resolution and sky coverage. With an FOV covering 25% of the sky, COSI aims to study the 511 keV positron annihilation line along with measurements of other radioactive nuclei in the galaxy. COSI also aims to study the polarization of gamma-ray sources, and detect and localize multimessenger transients.

3.3 Potential with Daksha

Like the missions mentioned above, *Daksha* also has the potential to perform Compton imaging with its layered detector design. The dome structure of the external ME Packages gives it inherent all-sky sensitivity at all times, and information from several pairs of detectors could be utilized to reconstruct sources in the sky. However, since Compton imaging was not its primary purpose, contamination from the X-ray background would be a significant challenge. In both COMPTEL and IBIS, the detectors are passively shielded from unwanted photons using thick tungsten and lead elements, ensuring that the majority of photons incident on the second detector are scattered off the first one. This is not the case for *Daksha*, which means that the background must be overcome by other means. We are optimistic that integration over the five year mission lifetime will yield enough signal.

4 Simulations

The simulations are done using GEANT4, and the details of the mass model and data interfacing are detailed in the BTP I report. The work done during BTP I involved

addition of pixellated HE detectors and the development of auxiliary classes to handle output data. The GEANT simulations generate a single output FITS file with two tables - one for the ME detectors and one for the HE detectors.

This raw simulation output is then processed using a Python script to convert the data into a realistic time-tagged event (TTE) format that would be generated by the actual mission. Briefly, this includes the following steps:

1. **Assigning timestamps to events**
   The `eventIDs` available in the raw data are used to assign timestamps to each event. The `eventID` is a unique identifier for each source photon that is generated in the simulation.The timestamps are assigned by assuming the arrival of photons to be a Poisson process with a constant average rate. These timestamps are then binned to the time resolutions of the detectors (10 μs for HE and 1 μs for ME) to create the TTE data.

2. **Assigning physical locations to events**
   Positional information is essential to the reconstruction process. This requires a mapping of the hierarchical IDs identifying each pixel to a physical location in the global frame of the mass model. A lookup table is used to convert these IDs to physical locations for ME and HE detections.

3. **Adding effects of energy resolution**
   In order to add the effects of energy resolution, the ME and HE energy deposits are perturbed by random offsets sampled from normal distributions with standard deviations of 10% and 7% of the original values respectively. These new values are stored in the same `edep` columns. Only entries with energy deposits $20 < E < 200$ keV are considered for the ME events data, and $100 < E < 1000$ keV for the HE events data. This is done to emulate the energy ranges of the actual detectors.

5 Methodology

Once the data is processed, the next step is to identify Compton events and reconstruct the source.

5.1 Event Selection

Events are selected primarily using the timestamps. ME events that occur in the same 10 μs time bin (this is the time resolution of the HE detectors, as discussed earlier) of

the HE detectors are considered to be coincident with the HE event occurring in that bin. Any simultaneous detection in two or more ME pixels are discarded, as these are very likely to be internal Compton scatters. If a HE time bin contains several distinct HE and ME events, all possible pairs are considered for reconstruction. This is done to ensure that no true pairs are missed, but it also means that more chance coincidences would be included. Whether or not this is the best approach is a question that needs to be addressed in the future.

For each Compton pair, we know the energy deposits in the ME and HE detectors (E_1 and E_2 respectively), and the interaction positions ($\vec{r}_1$ and $\vec{r}_2$ respectively). The vector $\vec{r}_{\text{scatt}}$ corresponds to the back-projected direction of the scattered photon, and is given by:

$$\vec{r}_{\text{scatt}} = \vec{r}_1 - \vec{r}_2 \tag{2}$$

The scattering angle ϕ can be determined from the energy deposits using the Compton formula:

$$\frac{1}{E_2} - \frac{1}{E_1 + E_2} = \frac{1}{m_e c^2}(1 - \cos\phi) \tag{3}$$

$$\implies \cos\phi = 1 - E_0 \left(\frac{1}{E_1 + E_2} - \frac{1}{E_2} \right) \tag{4}$$

$$\implies \phi = \cos^{-1}\left(1 - E_0 \left(\frac{1}{E_1 + E_2} - \frac{1}{E_2} \right) \right) \tag{5}$$

Where $E_0 = m_e c^2$ is the rest energy of the electron. Now, for each pair we have a back-projected scattered photon vector $\vec{r}_{\text{scatt}}$ and a scattering angle ϕ. This is enough information to constrain the incident photon vector to a cone. As discussed earlier, the intersection of many such cones can be used to reconstruct the source.

Note that this expression opens up a way to reject chance coincidences which yield unphysical scattering angles. Ensuring $\phi < 90^\circ$ (since HE detectors are 'below' the scatterers) will thus eliminate some of these events. Events can be filtered further by imposing cuts due to the geometry of the detectors. For example, in the case of the `ME1-HE0` pair, for an on-axis incident photon, the scattering angle must be less than 52° for detection to be geometrically possible.

5.2 Error due to energy resolution

As I demonstrated in my previous report, the energy resolution errors of each detector contributes to an error in the scattering angle. This error is given by:

$$\Delta\phi_{\text{ene}} = \frac{E_0}{\sin\phi}\sqrt{\left(\frac{1}{E_2^2} - \frac{1}{(E_1+E_2)^2}\right)^2 (\Delta E_2)^2 + \frac{(\Delta E_1)^2}{(E_1+E_2)^4}}$$

Now, substituting the energy resolution errors as $\Delta E1 = \eta_{\text{ME}} E_1$ and $\Delta E2 = \eta_{\text{HE}} E_2$, we get:

$$\Delta\phi_{\text{ene}} = \frac{E_0}{\sin\phi}\sqrt{\left(\frac{1}{E_2^2} - \frac{1}{(E_1+E_2)^2}\right)^2 (\eta_{\text{ME}} E_1)^2 + \frac{(\eta_{\text{HE}} E_2)^2}{(E_1+E_2)^4}} \tag{6}$$

As discussed earlier, $\eta_{\text{ME}} = 0.1$ and $\eta_{\text{HE}} = 0.07$. Clearly, this quantity has a strong dependance on the scattering angle as well as energy.

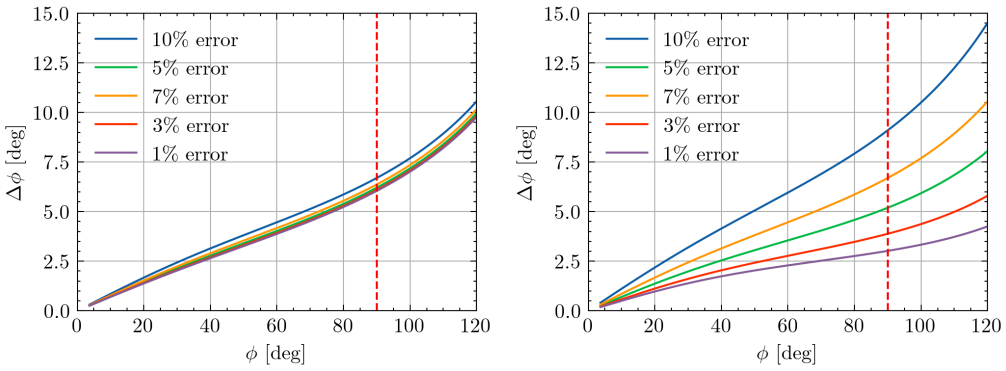

(a) Uncertainty in the Compton scattering angle $\Delta\phi$ as a function of ϕ for different values of the ME energy resolution error, for an incident photon energy of 500 keV. We see very little variation with the energy resolution.

(b) Uncertainty in the Compton scattering angle $\Delta\phi$ as a function of ϕ for different values of the HE energy resolution error, for an incident photon energy of 500 keV. We see significant variation with the energy resolution in this case.

5.3 Error due to position resolution

Due to uncertainty in the position of HE events, the back-projected scattered photon vector $\vec{r}_{\text{scatt}}$ is also uncertain. This uncertainty is due to the position resolution of the SiPMs, which is 1 cm and can be propagated to the scattering angle to give:

$$\Delta\phi_{\text{pos}} = \frac{d_{\text{pix}}(\vec{r}_{\text{norm}} \cdot \vec{r}_{\text{scatt}})}{|\vec{r}_{\text{scatt}}|^2}$$

Thus, we have both components for the error, and the total error can be obtained by adding them in quadrature.

$$\Delta\phi_{\rm tot} = \sqrt{(\Delta\phi_{\rm pos})^2 + (\Delta\phi_{\rm ene})^2}$$

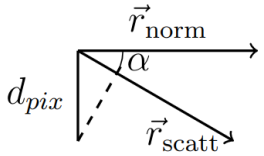

Figure 6

5.4 Reconstruction

Now, for each pair of events, we have the back-projected scattered photon vector $\vec{r}_{\rm scatt}$, a scattering angle ϕ and an associated error of $\Delta\phi_{\rm tot}$. To reconstruct the source, we can draw rings of with half angle ϕ around the back-projected scattered photon vector in spherical polar coordinates. In order to encode the uncertainty, the rings should have a gaussian profile in the half angle, with a standard deviation of $\Delta\phi_{\rm tot}$.

5.5 Visualization

This task was done with the healpy (Zonca et al., 2019) Python library library which is based on HEALPix (Górski et al., 2005). It has inbuilt functions for efficient visualization and manipulation of data on the sphere.

1. First, a function is called to generate a HEALpix map of ring about the z axis. This is because it is simpler to find the angle from the axis in this case, as its simply the colatitude. A range of half angles are generated from $\theta_0 - 3\sigma$ to $\theta_0 + 3\sigma$ with 30 steps. The magnitude profile with respect to θ is a gaussian, given by

   $$m(\theta) = \frac{1}{\sigma\sqrt{2\pi}} \exp\left(-\frac{(\theta-\theta_0)^2}{2\sigma^2}\right)$$

   This magnitude is evaluated for the 30 steps, and for each axial angle θ, a ring is generated with magnitude $m(\theta)$ over the range of longitudes $0 - 2\pi$.

2. Next, the rings thus generated are rotated to the correct axis. This is done by using in-built healpy functions that rotate maps in the spherical harmonic space.

3. This procedure is repeated for all pairs, and the maps thus obtained are added to each other.

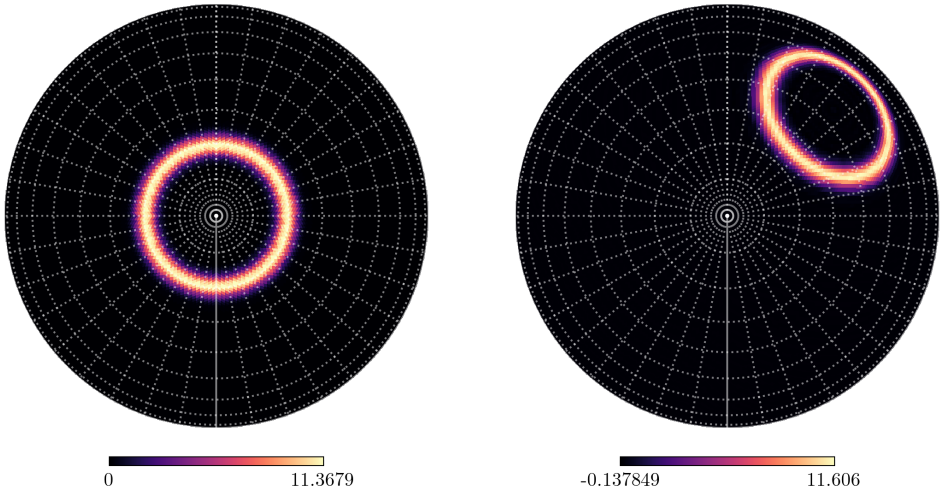

(a) Ring generated for $\theta_0 = 20°$, $\sigma = 2°$ (b) Rotated to $\theta = 45°$, $\phi = 225°$

Figure 7: Orthographic projection centred at $(\theta, \phi) = (90°, 0°)$

6 Compton Data Space

A Compton telescope measures the energies and positions of each interaction in the detectors. This raw data space is high dimensional and difficult to analyze, moreover, it contains more information than is strictly necessary for image reconstruction and data analysis. There is thus a need for a reduced data space that can be used to analyze the data more effectively.

The Compton Data Space (CDS), originally pioneered for the COMPTEL mission (Knödlseder et al., 1999), is a standardized representation of Compton scattering information. It is a three dimensional reduced data space storing the Compton scattering angle (ϕ) along with the polar and azimuthal angles of the scattered photon, χ and ψ (Kierans et al., 2022). Figure 8a denotes these. These angles define an orthogonal data space which makes it easy to analyze Compton data and has been used by several missions since COMPTEL.

Each reconstructed Compton event can be represented as a point in the CDS. This is in contrast to the image space, where each event is represented as an event circle. Since the Compton scattering angle is equal to the deviation between the incident and scattered photon vectors, properly reconstructed events lie along the surface of a cone that has its apex at the source location in the $\chi - \psi$ plane and an opening angle of 90° in the ϕ direction. Note that there will be deviations from this ideal case due to the energy and position resolution errors. This cone in the CDS is therefore a useful way to represent the point spread function (PSF) of a Compton telescope. Figure 8b illustrates this.

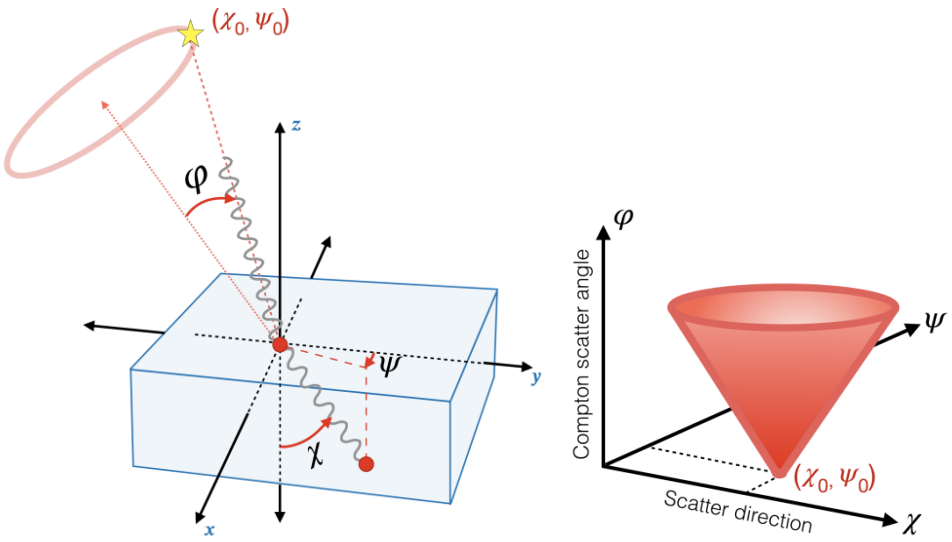

(a) Definition of the CDS angles χ, ψ and ϕ (b) PSF in the CDS is a cone

Figure 8: Compton Data Space. Image source: Kierans et al. (2022)

The density of events along the cone follows Compton kinematics and the Klein-Nishina cross section. For example, the events near the apex of the cone have smaller Compton scattering angles and are likely to be populated by higher energy photons. The geometry of detectors also plays a role in the distribution of events, as certain scattering directions are geometrically forbidden due to the physical arrangement of the detectors.

6.1 Angular Resolution

The Compton scatter angle is effectively encoded twice in the CDS, once as the ϕ coordinate of the event, and once as the deviation between the known incidence direction and the back-projected scattered photon direction. This apparent redundancy helps characterize how accurately the Compton telescope can measure the scattering angle. The angular resolution of the telescope can be quantified by the width of the cone wall in the CDS.

A common proxy for this is the Angular Resolution Measure (ARM), which can be obtained from a 2D projection of the CDS. This is obtained by defining the quantities ϕ^{kin} and ϕ^{geo} as the Compton scattering angles predicted by Compton kinematics and the geometry of the detectors respectively. The ARM for each event is then defined as the difference between these two quantities.

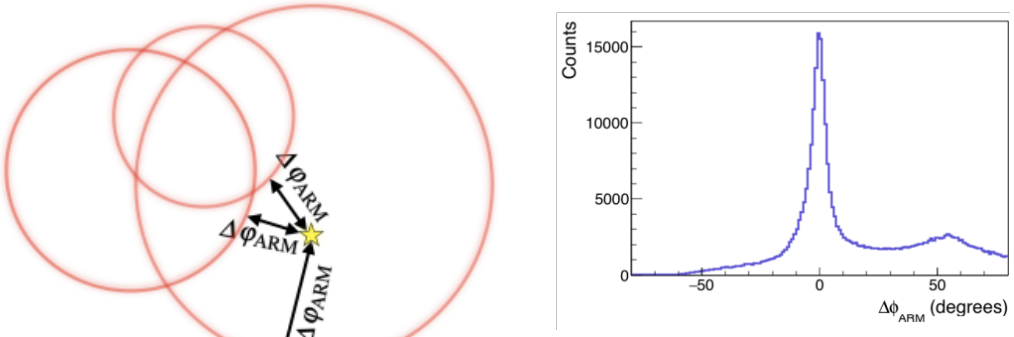

(a) ARM in image space

(b) ARM histogram of COSI for a 511 keV lab source

Figure 9: Image source: Kierans et al. (2022)

$$\Delta\phi_{\mathrm{ARM}} = \phi^{\mathrm{geo}} - \phi^{\mathrm{kin}} \tag{7}$$

In the image space, this quantity is equivalent to the shortest angular distance between the event circle and the true source location, as shown in Figure 9a. The ARM can be used to quantify the angular resolution of the telescope, and is a useful metric for comparing different Compton telescopes. The angular resolution of a Compton telescope is defined as the FWHM of the ARM distribution. For correctly reconstructed events, the ARM should be zero or close to it, and the distribution should be centered around zero. Figure 9b shows a typical ARM histogram for the COSI mission, measured using a far-field laboratory source. This shows that the mission has a angular resolution of 6°. There are often tails/off-axis peaks in the ARM distribution due to incorrectly reconstructed events and chance coincidences, and these can be rejected by imposing cuts on the ARM.

7 Simulating Crab Nebula

In the previous report, I discussed the results of simulations from monoenergetic photons. In this section, I will discuss the results of simulations from a more realistic source, the Crab nebula. The Crab nebula is a well-known source of gamma rays, and is a bright source in the MeV range. The spectrum of the Crab nebula is well known, and is well described by a power law with an average index of -2.1 over the 1 keV - 1

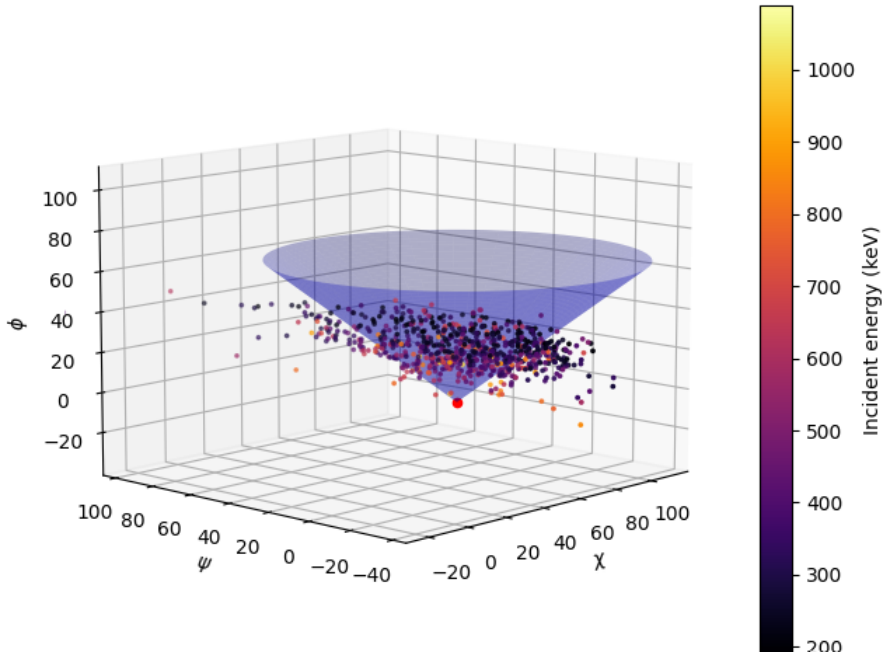

Figure 10: PSF of the ME1−HE0 pair in CDS, demonstrating the key features that were discussed in Section 6. The apex of the cone is marked by the red point, which is at $(45°, 0°)$, the source location of this simulation. Only one side of the cone is populated with events, as the detector geometry only permits a small range of polar angles for the scattering vector - this makes the distribution resemble a plane. Moreover, we observe that events closer to the apex are more likely to have a higher energy.

MeV range (Willingale et al., 2001) and a flux of $N_0 = 9.59$ ph/keV/cm^2/s at 1 keV. The photon spectrum is thus given by the following equation:

$$N(E) = N_0 \left(\frac{E}{1 \text{ keV}} \right)^{\alpha}$$

Similar to the previous monoenergetic simulations, a circular source plane is defined in GEANT4, and the photons are generated with energies drawn from this spectrum. The photons are then propagated through the mass model, and the data is processed as described before. The exposure time is set to 300 ks (∼3.5 days) to simulate a long exposure.

7.1 Compton Data Space Analysis

After reconstructing events with the ME1−HE0 detector pair, we find 2217 Compton pairs in this 300 ks exposure, corresponding to a rate of 7.4 pairs per kilosecond. Figure 10 shows the PSF for this system in the CDS. There are many poorly reconstructed

and chance-coincidence events, as evidenced by the large spread of events beyond the walls of the cone. The number of true Compton pairs in this duration is 844, which is about 38% of the total pairs.

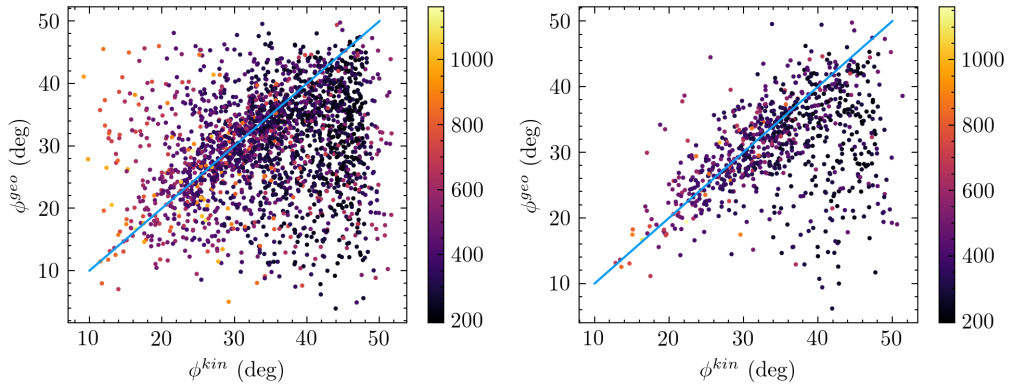

(a) Projected PSF for timed events

(b) Projected PSF for true events

Figure 11: In the plots above, the blue line denotes $\phi^{\text{kin}} = \phi^{\text{geo}}$ along which properly reconstructed events must lie. Evidently, the plot for events selected by timing contains a large amount of background contamination due to chance coincidences. The 'true' events also seem to contain some erroneous reconstructions, likely due to incompletely absorbed photons that could not be excluded.

The full CDS is impractical to analyze visually, so Figure 11 shows a 2D projection of the CDS in terms of the geometric and reconstructed scattering angles, as discussed in Section 6.1. This projected PSF can also be created for true Compton events that are chosen by utilizing `eventIDs` supplied by GEANT4 to see the theoretical best performance that could be achieved with perfect event selection. As expected, the true events are more tightly clustered around the line $\phi^{\text{kin}} = \phi^{\text{geo}}$, and the spread of events is lower.

7.2 Angular Resolution

As discussed in Section 6.1, the angular resolution of a Compton telescope can be quantified by the FWHM of the ARM distribution. The ARM distribution for the timed and true events is shown in Figure 12a. For the timed events, the ARM distribution has a peak centered around zero, as expected, but has significant contamination due to chance coincidences and poorly reconstructed events. This distribution can be fitted well to a bimodal Gaussian distribution, with the stronger peak around 0° corresponding to the true events, and the weaker, broader peak corresponding to the background.

The ARM histogram for 'true' events has fewer spurious events, and indicates an FWHM of 8°, which can be interpreted as a lower limit for the angular resolution of

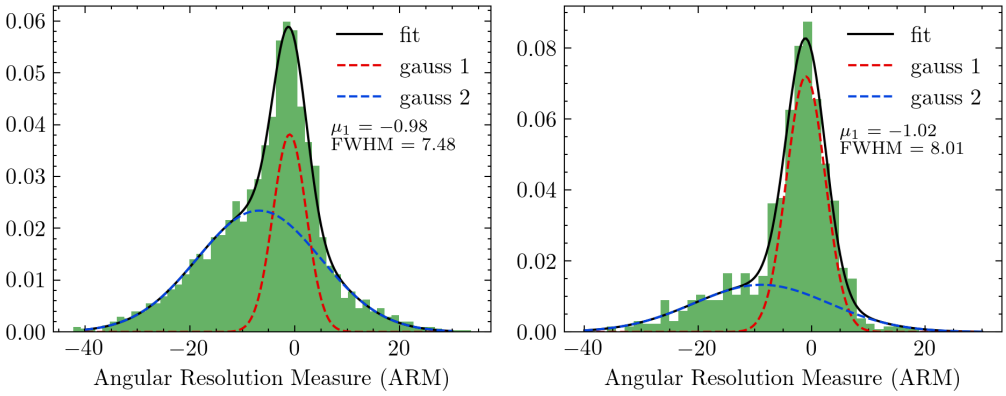

(a) ARM histogram for timed events

(b) ARM histogram for true events

the mission. It also shows that nearly all the true events are located within 10° of zero. This suggests that applying a cut on the ARM at 10° for timed reconstruction would eliminate most of the background events, while retaining a most of the true events. This ARM cut significantly improves the contrast of images (as seen in Figures 13 and 14), and effectively gives a practical angular resolution of $\sim 10^\circ$ for the mission. Of course, this condition inherently assumes that the source location is known. In order to use this in practice, we would have to computationally image small patches of the sky and piece together an all-sky image to search for sources.

7.3 Back-projected Images

The images below are for a 60 ks exposure, and the source location is $(\theta, \phi) = (45°, 0°)$ marked with $\times$.

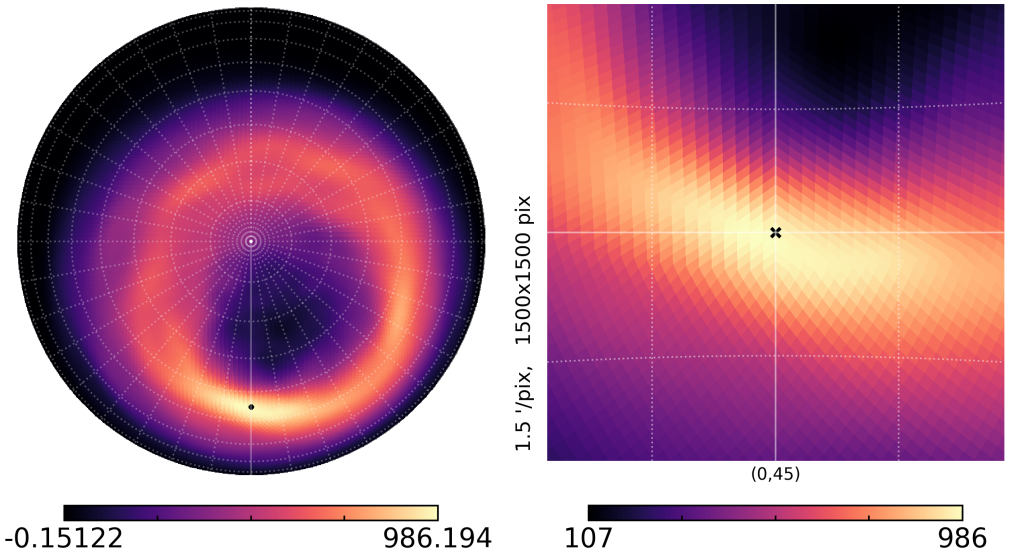

Figure 13: Localization without ARM cut applied.

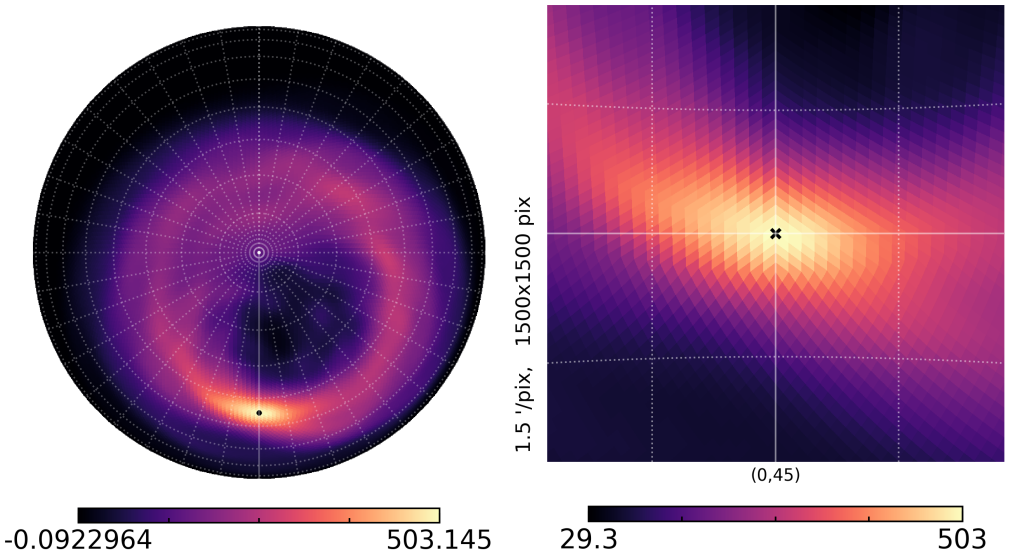

Figure 14: Localization with ARM cut applied.

8 Including Background

All of the analysis done so far has been on simulated data from a source. However, the actual mission will have to deal with a significant background from cosmic rays and the cosmic X-ray background. The cosmic X-ray background is a significant source of background in the MeV range, and is a major challenge for Compton telescopes. The CXB is also reflected off the Earth's atmosphere, making the background anisotropic and dependent on the satellite pointing and the Earth's position. In addition to this, we have to deal with the hard X-ray albedo of the Earth, which is generated by the interaction of cosmic rays with the atmosphere.

8.1 Simulations

The background simulations for each component were done separately, using spectra from Cumani et al. (2019). The simulations are done using an uniform spherical source that encloses the entire mass model. The angular spread is limited so that most photons are incident on the satellite and aren't wasted. We assume the satellite to be pointed with the dome to the sky and the bus facing the earth. This makes it so that the CXB and primary particle background components (protons, alpha particles, electrons and positrons) would be shining on the dome, while the reflected CXB and hard X-ray albedo from Earth would shine from below. To simulate this anisotropy, the full spherical simulations are post-processed to only include events that originate from the desired solid angle range, which is decided by the satellites altitude. Figures 15a and 15b show the input spectra used for each photon background component and each particle type.

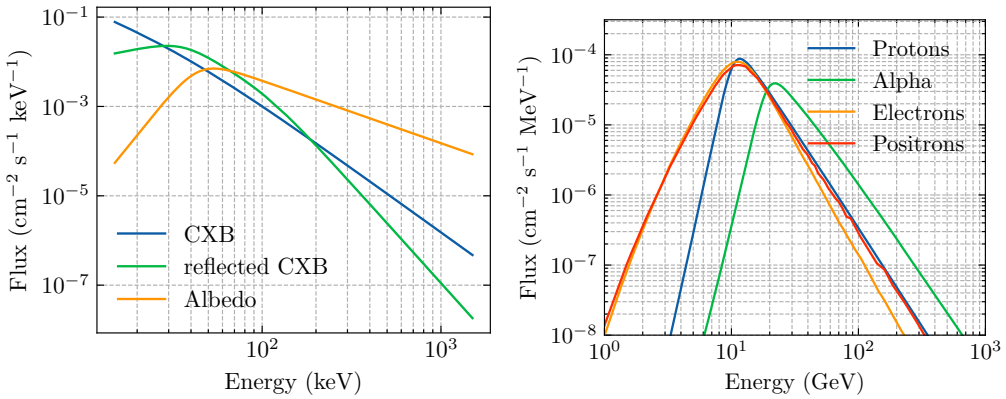

(a) Photon background components (b) Particle background components

Figure 15: Input spectra used for background simulations

8.2 Detected Background due to Photons

The detected background due to photons is shown in Figure 16. The background is clearly dominated by the CXB, which has a relatively flat spectrum and shines from the top of the satellite. The albedo and reflected CXB components shine from the bottom here and are significantly weaker, with CXB dominating over them by at least an order of magnitude at any given energy for the ME detector. In case of the HE detector, the harder albedo input spectrum overcomes the CXB, but is still weakened by the angular cuts that are implemented.

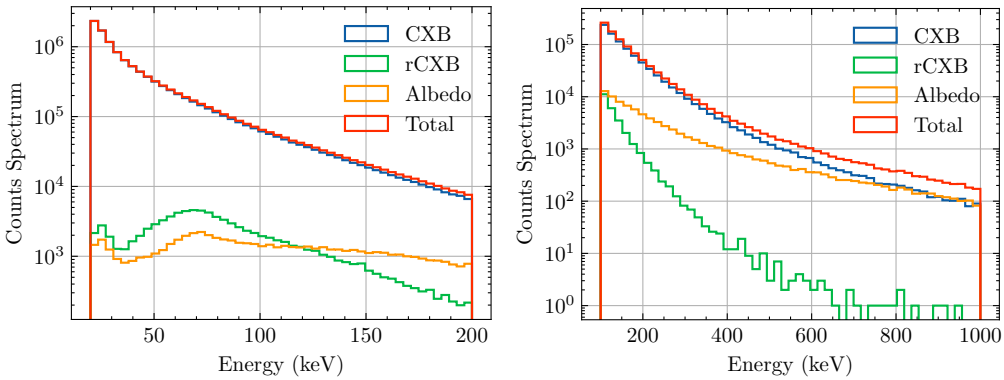

(a) Detected photon background for ME (b) Detected photon background for HE

Figure 16: Detected background due to photons

The integrated count rate for the photon background is 1670 counts/s for the `ME0` (topward) detector, or a flux of 5.57 counts/cm^2/s. For the `HE0` (bottomward) detector, the count rate is 147 counts/s, or a flux of 0.37 counts/cm^2/s. The background is significantly higher for the ME detector, which is expected due to the higher sensitivity in this energy range.

Component	Flux (count/cm^2/s)
CXB	5.49
Albedo	0.03
Reflected CXB	0.04
Photon Total	5.56
Proton	0.029
Alpha	0.004
Electron	0.002
Particle Total	0.035

Table 1: Fluxes for ME detector

Component	Flux (count/cm^2/s)
CXB	0.33
Albedo	0.03
Reflected CXB	0.03
Photon Total	0.39
Proton	0.044
Alpha	0.008
Electron	0.003
Particle Total	0.055

Table 2: Fluxes for HE detector

8.3 Detected Background due to Particles

The detected background due to particles is shown in Figure 17. The background is dominated by protons, with the total contribution being relatively flat across the energy range for both detectors. The particles are assumed to be shining from the top of the satellite, only from the region that is unobstructed by the Earth.

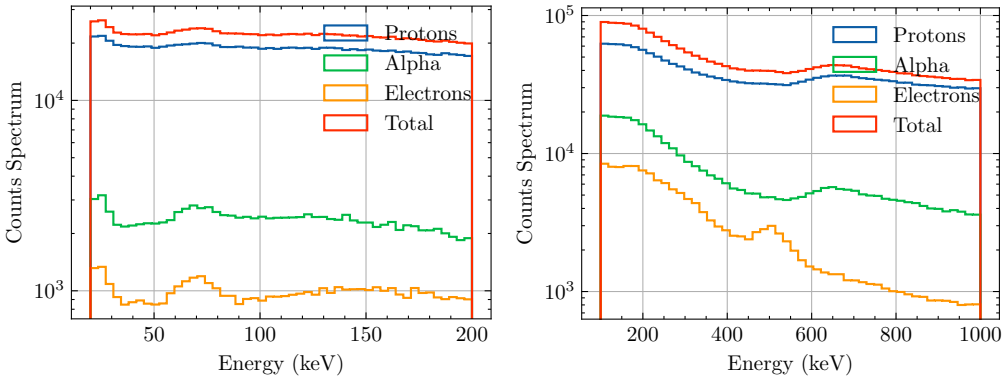

(a) Detected particle background for ME (b) Detected particle background for HE

Figure 17: Detected background due to particles

The integrated flux rates for all the particles combined is 0.0056 counts/cm^2/s for the ME detector, and 0.0092 counts/cm^2/s for the HE detector. Being a scintillator type detector, the HE detector is more sensitive to particles, and this is reflected in the higher background rate. The particle background is significantly lower than the photon background for ME detectors, but is comparable for the HE detector.

9 Conclusion and Future Work

Through this B.Tech project, I have gained a deep understanding of the principles of Compton imaging and the challenges faced by Compton telescopes. I have also gained experience in using GEANT4 for simulations and in analyzing the data generated by these simulations. The work done in this project has also been a significant step towards generating flight-like data for the *Daksha* mission, including detailed and realistic background simulations.

I have successfully demonstrated basic event selection and imaging techniques for Compton telescopes, and have shown that the *Daksha* mission has the potential to perform Compton imaging. The ARM distribution for the mission has been calculated, and the angular resolution has been estimated to be $\sim 10^\circ$. However, the background from cosmic rays and the cosmic X-ray background outshines the source signal by at

least an order of magnitude, and this will be a significant challenge for the mission. To solve this problem, Compton telescopes use deconvolution techniques to separate the source signal from the background. The measured data is assumed to be the result of a convolution with the detector response in the CDS Kierans et al. (2022). This can be written as

$$D(\chi, \psi, \phi) = R(\chi, \psi, \phi; l, b) * I(l, b) + B(\chi, \psi, \phi)$$

This equation convolves the source information in the sky coordinate space with the detector response, R, which also depends on the sky location. If this response function can be computed, iterative methods can be used to invert this equation and obtain the true source information. One such technique commonly used in Compton telescopes is the List Mode Maximum-Likelihood Expectation Maximization (LM-ML-EM) method (Kierans et al., 2022). I am currently working on adapting such imaging algorithms that have already been implemented by the COSI team as a part of the `cosipy` (Martinez, 2023) package that is currently under development.

10 Acknowledgements

I would like to thank Profs. Gulab Dewangan and Varun Bhalerao for guiding me through this project and providing me with the opportunity to work on this exciting mission. I would also like to thank Israel Martinez from NASA/GSFC for his guidance on the imaging deconvolution tools implemented within `cosipy` and Dr. Sujay Mate for helping me with the background simulations and GEANT4 development work.

References

Agostinelli, S., Allison, J., Amako, K., et al. 2003, Nuclear Instruments and Methods in Physics Research Section A: Accelerators, Spectrometers, Detectors and Associated Equipment, 506, 250, doi: https://doi.org/10.1016/S0168-9002(03)01368-8

Bhalerao, V., Vadawale, S., Tendulkar, S., et al. 2022, Daksha: On Alert for High Energy Transients. https://arxiv.org/abs/2211.12055

Cumani, P., Hernanz, M., Kiener, J., Tatischeff, V., & Zoglauer, A. 2019, Experimental Astronomy, 47, 273–302, doi: 10.1007/s10686-019-09624-0

Forot, M., Laurent, P., Lebrun, F., & Limousin, O. 2007, The Astrophysical Journal, 668, doi: 10.1086/521325

Górski, K. M., Hivon, E., Banday, A. J., et al. 2005, ApJ, 622, 759, doi: 10.1086/427976

Kierans, C., Takahashi, T., & Kanbach, G. 2022, Compton Telescopes for Gamma-Ray Astrophysics (Springer Nature Singapore), 1–72, doi: 10.1007/978-981-16-4544-0_46-1

Knödlseder, J., Dixon, D., Bennett, K., et al. 1999, A&A, 345, 813, doi: 10.48550/arXiv.astro-ph/9903172

Martinez, I. 2023, in Proceedings of 38th International Cosmic Ray Conference — PoS(ICRC2023), ICRC2023 (Sissa Medialab), doi: 10.22323/1.444.0858

Schönfelder, V., Diehl, R., Lichti, G. G., et al. 1984, IEEE Transactions on Nuclear Science, 1, 766, doi: 10.1109/TNS.1984.4333363

Venugopal, V., & Bhagdikar, P. 2013, Physics Education, 29, 35

Willingale, R., Aschenbach, B., Griffiths, R. G., et al. 2001, A&A, 365, L212, doi: 10.1051/0004-6361:20000114

Zonca, A., Singer, L., Lenz, D., et al. 2019, Journal of Open Source Software, 4, 1298, doi: 10.21105/joss.01298